First principles predictions of thermophysical properties of refrigerant mixtures

Mark T. Oakley, Hainam Do, Jonathan D. Hirst, and Richard J. Wheatley

Citation: The Journal of Chemical Physics **134**, 114518 (2011); doi: 10.1063/1.3567308
View online: http://dx.doi.org/10.1063/1.3567308
View Table of Contents: http://scitation.aip.org/content/aip/journal/jcp/134/11?ver=pdfcov
Published by the AIP Publishing

First principles predictions of thermophysical properties of refrigerant mixtures

Mark T. Oakley, Hainam Do, Jonathan D. Hirst, and Richard J. Wheatley[a)]
School of Chemistry, University of Nottingham, University Park, Nottingham NG7 2RD, United Kingdom

(Received 13 January 2011; accepted 25 February 2011; published online 17 March 2011)

We present pair potentials for fluorinated methanes and their dimers with CO_2 based on *ab initio* potential energy surfaces. These potentials reproduce the experimental second virial coefficients of the pure fluorinated methanes and their mixtures with CO_2 without adjustment. *Ab initio* calculations on trimers are used to model the effects of nonadditive dispersion and induction. Simulations using these potentials reproduce the experimental phase-coexistence properties of CH_3F within 10% over a wide range of temperatures. The phase coexistence curve of the mixture of CH_2F_2 and CO_2 is reproduced with an error in the mole fractions of both phases of less than 0.1. The potentials described here are based entirely on *ab initio* calculations, with no empirical fits to improve the agreement with experiment. © *2011 American Institute of Physics*. [doi:10.1063/1.3567308]

I. INTRODUCTION

Supercritical carbon dioxide is a novel solvent that has attracted a great deal of attention.[1] A property of interest is the unusually high solubility of fluorinated compounds in supercritical CO_2. Simulations can provide some insight into the intermolecular interactions that give rise to this unusual solubility. Mixtures of hydrofluorocarbons (HFCs) and CO_2 are possible replacements for ozone-depleting refrigerants. Knowledge of the phase-coexistence properties of these mixtures is vital to optimize their performance in refrigeration cycles.

Simulations can provide new information on the thermophysical characteristics of a system and the relationship to its microscopic structure. Such simulations often use empirical potentials, where the parameters are fitted to reproduce experimental results. Gibbs ensemble Monte Carlo simulations of CH_2F_2 using a five-center charge plus Lennard-Jones potential reproduce the phase-coexistence curve.[2] This potential also reproduces the properties of the mixture of CH_2F_2 with CO_2.[3]

Ab initio calculations are an alternative way to generate potentials and have the advantage of being able to model systems where no experimental data are available. *Ab initio* potential energy surfaces for all of the fluorinated methane dimers have been calculated at the HF/6-31+G* level, with some additional calculations using the MP2 method.[4] These potentials have been used to calculate the free energy of solvation of all of these compounds in CO_2,[5] but no experimental data are available to check the results of these simulations. The potential energy surface of CH_3F has been generated using symmetry adapted perturbation theory (SAPT) calculations.[6] The resulting potential reproduces the phase coexistence curve well but is only calculated with a small aug-cc-pVDZ basis set. We have shown that simulations of CO_2 using a pair potential calculated with a small basis set fortuitously obtain the correct phase-coexistence curve by underestimating the pair binding energy and neglecting the repulsive three-body dispersion energy.[7]

Potentials derived entirely from *ab initio* calculations reproduce the phase-coexistence properties of CO_2 (Ref. 7) and CH_4 (Ref. 8) well, but only when all interactions that could affect the phase properties are included explicitly. In the case of CO_2 and CH_4, accurate pair potentials are too strongly bound and the correct phase properties are only obtained when the effect of three-body dispersion is also included. Here, we report simulations of fluorinated methanes using *ab initio* pair potentials and a correction for the three-body dispersion energy. We also model the effect of three-body induction, which is important when simulating polar molecules. Unless otherwise stated, all values quoted in this paper are in atomic units, with energies in hartree (E_h) and distances in Bohr (a_0).

II. POTENTIAL

The total energy of a dimer, trimer, or periodic box of molecules is assumed to be the sum of electrostatic, induction, dispersion, and exchange repulsion components,

$$U = U_{\text{elec}} + U_{\text{ind}} + U_{\text{disp}} + U_{\text{rep}}. \tag{1}$$

This is a convenient representation for fitting rather than a rigorous division. For example, the non-multipolar components of the electrostatic and induction energies are taken up by the dispersion and repulsion terms.

The electrostatic energy of a pair of molecules A and B is given by

$$U_{\text{elec},AB} = \sum_{a\in A}\sum_{b\in B}\left[\frac{q_a q_b}{r_{ab}} + \frac{q_a \mu_b R_{ab}}{r_{ab}^3} - \frac{q_b \mu_a R_{ab}}{r_{ab}^3} - \frac{3\mu_a R_{ab}\mu_b R_{ab}}{r_{ab}^5} + \frac{\mu_a \mu_b}{r_{ab}^3}\right], \tag{2}$$

where R_{ab} is a vector from atom a to atom b, with length r_{ab}. The atomic charges, q, and dipole moments, μ, are obtained from iterated stockholder atom calculations[9,10]

a)Electronic mail: richard.wheatley@nottingham.ac.uk.

TABLE I. Atomic coordinates calculated at the MP2/aug-cc-pVQZ level. Atomic charges, dipole moments and polarisabilities calculated at the HF/aug-cc-pVQZ level. All values are in atomic units.

	x	y	z	q	μ_x	μ_y	μ_z	α
CH_3F								
C	0.000	0.000	–1.406	0.170	0.000	0.000	0.170	11.663
F	0.000	0.000	1.218	–0.290	0.000	0.000	–0.070	4.175
H	1.946	0.000	–2.064	0.040	0.058	0.013	–0.004	0.000
H	–0.973	1.685	–2.064	0.040	–0.029	0.050	–0.004	0.000
H	–0.973	–1.685	–2.064	0.040	–0.029	–0.050	–0.004	0.000
CH_2F_2								
C	0.000	0.000	–1.054	0.548	0.000	0.000	0.185	7.604
F	0.000	–2.082	0.449	–0.297	0.000	0.019	0.012	4.234
F	0.000	2.082	0.449	–0.297	0.000	–0.019	0.012	4.234
H	1.719	0.000	–2.178	0.023	0.070	0.000	–0.027	0.000
H	–1.719	0.000	–2.178	0.023	–0.070	0.000	–0.027	0.000

on single molecules (Table I). The HFC molecules in this study are all polar. Therefore, long-range electrostatic interactions cannot be ignored and Ewald summation techniques are used in all Monte Carlo simulations.[11]

The induction energy of a molecule, A, is given by

$$U_{\text{ind},A} = -\frac{1}{2}\sum_{a\in A}(\alpha_a F^2), \tag{3}$$

where F is the external field at a from the atomic charges and dipole moments on all other molecules in the system. The atomic polarizabilities, α, are obtained from *ab initio* calculations on single molecules[12] (Table I). A united atom representation is used, with the polarizabilities of the hydrogen atoms included in the nearest heavy atom, and the polarizabilities are spherically averaged. The induction energy is therefore calculated to second order in the field. An iterative treatment, where the induced dipoles polarize the surrounding molecules, is not used. The $U_{\text{ind},A}$ term includes both the additive and nonadditive induction energies.

The dispersion energy has two-body and three-body components. The two-body dispersion energy is given by

$$U_{2,\text{disp}} = \sum_{a\in A}\sum_{b\in B}\left[\frac{C^6_{ab}}{r^6_{ab}}\right]. \tag{4}$$

The C^6 coefficients are fitted to reproduce *ab initio* potential energy surfaces. Details of the fitting method and potential energy surfaces are given in Sec. III. A long-range correction is applied to account for all dimers whose separation is greater than a cutoff radius, r_{cut}:

$$U_{2,\text{disp},lr} = \frac{4}{3}\pi\rho C r^{-3}_{\text{cut}}, \tag{5}$$

where C is the total C^6 coefficient for a pair of molecules and ρ is the number density of the phase being simulated.

The three-body dispersion energy is given by the Axilrod–Teller equation[13]

$$U_{3,\text{disp}} = \frac{1}{6}\sum_{a,b,c}\nu_{abc}(1+3\cos\theta_a\cos\theta_b\cos\theta_c)r^{-3}_{ab}r^{-3}_{ac}r^{-3}_{bc}, \tag{6}$$

where θ_a, θ_b and θ_c are the angles in the triangle abc, and these atoms are all in different molecules. The Axilrod–Teller coefficients, ν, are fitted to reproduce *ab initio* nonadditive dispersion energies.

A long-range correction is applied to account for all trimers whose separation is greater than a cutoff distance, r_{cut},

$$U_{3,\text{disp},lr} = \frac{\pi^2\rho^2\nu}{r^3_{\text{cut}}}\left[\frac{11}{9} - \frac{s}{r_{\text{cut}}}\right], \tag{7}$$

where s is a collision radius, which is set to 2.5 a_0 for all molecules considered here.[14]

The two-body exchange repulsion energy is fitted by

$$U_{\text{rep}} = \sum_{a\in A}\sum_{b\in B}\left[\frac{C^n_{ab}}{r^n_{ab}}\right]. \tag{8}$$

In our work on CH_4,[8] we found that a Lennard-Jones 6–12 potential makes the repulsive wall too steep for interactions involving hydrogen atoms. Therefore, $n = 8$ is used for any pairs including a hydrogen atom and $n = 12$ is used for all other interactions. The C^8 and C^{12} parameters are fitted to reproduce dimer potential energy surfaces. Details of these calculations are in Sec. III.

III. COMPUTATIONAL METHODS

Potential energy surfaces for the CH_3F and CH_2F_2 dimers and their dimers with CO_2 are calculated with the MOLPRO package[15] using second-order Møller–Plesset perturbation theory (MP2) and the aug-cc-pVDZ basis set. Counterpoise correction is used to remove the basis set superposition error. The geometries are generated by varying the intermolecular separation in steps of 0.5 a_0 and the intermolecular angles in steps of $\pi/6$ rad. Any geometries with H–H separations shorter than 2.5 a_0, F–X separations closer than 4.0 a_0, or any other separations shorter than 5.0 a_0 are excluded, as are those where all pairs are separated by more than 13 a_0. This gives a total of 23 356 points for the CH_3F dimer, 69 959 for the CH_2F_2 dimer, 63 708 for CH_3F/CO_2, and 85 777 for CH_2F_2/CO_2.

A subset of 1000 points is chosen from each of these potential energy surfaces for higher-level calculations. The

TABLE II. Parameters in the HFC dimer pair potentials calculated at the CCSD(T)/CBS level. The Boltzmann-weighted rms error, σ_{Boltz}, is calculated for the potential energy surface at the MP2/aug-cc-pVDZ level. All quantities are in atomic units.

	Nonpolarizable		Polarizable	
Molecule	CH_3F	CH_2F_2	CH_3F	CH_2F_2
C^6_{CC}	36.8	–88.1	24.6	–100
C^6_{CF}	–12.4	1.64	–6.55	6.92
C^6_{CH}	–64.8	–39.3	–61.7	–36.1
C^6_{FF}	–26.8	–17.5	–25.0	–16.9
C^6_{FH}	–2.64	–4.78	–2.16	–4.67
C^6_{HH}	8.59	2.09	8.44	2.46
C^{12}_{CC}	1.78×10^6	3.26×10^6	2.02×10^6	3.65×10^6
C^{12}_{CF}	6.14×10^5	5.21×10^5	6.11×10^5	5.18×10^5
C^8_{CH}	1.07×10^3	7.33×10^2	1.02×10^3	6.80×10^2
C^{12}_{FF}	3.34×10^5	2.78×10^5	3.41×10^5	2.79×10^5
C^8_{FH}	1.80×10^2	1.90×10^2	1.76×10^2	1.89×10^2
C^8_{HH}	-3.22×10^1	2.07×10^1	-3.11×10^1	1.81×10^1
$\sigma_{\text{Boltz}}/\mu E_h$	240	219	242	221

structures are selected at random and accepted with a probability proportional to $1/(E+E')^2$, where E is the MP2/aug-cc-pVDZ dimer interaction energy and E' is 5 mE_h. This not only tends to select points near the energy minimum but also provides some coverage of the repulsive wall. The energies of these dimers are calculated at the MP2/aug-cc-pVTZ and MP2/aug-cc-pVQZ levels. An extrapolation to the complete basis set limit is performed by an exponential fit to the double-, triple- and quadruple-zeta values,[16] using

$$U_X = U_\infty + Be^{-CX}, \tag{9}$$

TABLE III. Parameters in the HFC/CO_2 pair potentials calculated at the CCSD(T)/CBS level. The Boltzmann-weighted rms error, σ_{Boltz}, is calculated for the potential energy surface at the MP2/aug-cc-pVDZ level. The carbon atom in CO_2 is labeled as C′. All quantities are in atomic units.

	Nonpolarizable		Polarizable	
Molecule	CH_3F/CO_2	CH_2F_2/CO_2	CH_3F/CO_2	CH_2F_2/CO_2
$C^6_{CC'}$	–95.2	–97.1	–97.4	–60.3
C^6_{CO}	–27.9	–20.3	–26.5	–33.5
$C^6_{FC'}$	–7.94	–6.94	–4.08	–15.2
C^6_{FO}	–15.1	–13.6	–13.2	–10.6
$C^6_{HC'}$	–0.274	0.646	1.93	–2.81
C^6_{HO}	–11.5	–13.7	–11.2	–12.7
$C^{12}_{CC'}$	2.38×10^6	1.94×10^6	2.33×10^6	1.62×10^6
C^{12}_{CO}	1.12×10^6	9.88×10^5	1.03×10^6	1.07×10^6
$C^{12}_{FC'}$	2.33×10^5	3.78×10^5	3.08×10^5	4.06×10^5
C^{12}_{FO}	4.68×10^5	3.85×10^5	4.00×10^5	3.77×10^5
$C^8_{HC'}$	2.20×10^2	1.91×10^2	1.67×10^2	2.28×10^2
C^8_{HO}	3.22×10^2	3.42×10^2	3.47×10^2	3.33×10^2
$\sigma_{\text{Boltz}}/\mu E_h$	249	230	250	226

TABLE IV. Axilrod–Teller coefficients (in atomic units) and density-dependent terms for nonadditive dispersion energy calculations.

	CH_3F	CH_2F_2
ν_{CCC}	0.0	0.0
ν_{FFF}	64.7	61.3
ν_{HHH}	14.2	10.4
ν	1435	1814
RMS fit error/μE_h	2.4	1.9
k/E_h Å$^{7.5}$	7.15	8.66

where X is the cardinal number of the basis set (2, 3, or 4 for double-, triple-, or quadruple-zeta) and B and C are fitted parameters.

Coupled cluster calculations have a better treatment of the correlation energy than MP2, but are much more computationally expensive and impractical with basis sets larger than aug-cc-pVTZ. Pair energies are evaluated at the CCSD(T)/aug-cc-pVTZ level and an estimate of the complete basis coupled cluster energy is obtained by assuming

$$U_{\text{CCSD(T)/CBS}} = U_{\text{CCSD(T)/aug-cc-pVTZ}} - U_{\text{MP2/aug-cc-pVTZ}} + U_{\text{MP2/CBS.}} \tag{10}$$

In our previous work on CO_2, there is little difference between the dimer interaction energies calculated at the MP2 and CCSD(T) levels. However, for the fluorinated methanes considered here, the CCSD(T)/aug-cc-pVTZ dimer interaction energies in geometries near the global minimum are about 250 μE_h more negative than the corresponding MP2/aug-cc-pVTZ energies.

Potentials are fitted for each of the MP2/aug-cc-pVDZ energy surfaces. For each dimer, we fit two potentials: nonpolarizable and polarizable. In the nonpolarizable potentials, $\alpha = 0$ on all atoms and the pair induction energy becomes part of the dispersion/exchange-repulsion fit. Simulations with these potentials only include pair induction effects. In the polarizable potentials the calculated atomic polarizabilities are used and the ensuing simulations include the effect of nonadditive induction.

The electrostatic and induction components of the energy are generated from the *ab initio* charges, dipole moments, and polarizabilities. These are subtracted from the total interaction energy to give a dispersion/repulsion energy, which is fitted by a Boltzmann-weighted least squares fit of the C^6, C^8, and C^{12} parameters. No constraints are applied to these parameters, and positive C^6 or negative C^8 and C^{12} parameters are allowed. In some geometries on the repulsive wall, this leads

TABLE V. Second virial coefficients of the CO_2 dimer. Virial coefficients are in cm^3 mol^{-1}.

T / K	Exp.[21]	Trappe-EH	CBS-ad
303.15	–118.8	–111.5	–118.2
313.15	–109.8	–103.4	–109.6
323.15	–103.6	–96.0	–101.8
333.15	–95.1	–88.9	–94.7
343.15	–89.5	–83.1	–88.1

TABLE VI. Second virial coefficients of the fluorinated methane dimers. Virial coefficients are in $cm^3\ mol^{-1}$.

	CH_3F		CH_2F_2	
T / K	Exp.[20]	Calc.	Exp.[21]	Calc.
303.15	–196.8	–192.7	–283.9	–282.8
313.15	–182.2	–178.9	–257.5	–260.6
323.15	–169.2	–166.5	–238.5	–240.9
333.15	–157.5	–155.3	–220.8	–223.3
343.15	–145.4	–145.1	–202.8	–207.5

to a positive $U_{2,\mathrm{disp}}$ or a negative U_{rep}. To prevent holes in the repulsive wall, short interatomic contacts are treated with a hard-sphere potential, with radii of 1.25 a_0 for H, 1.75 a_0 for F, and 1.9a_0 for all other atoms.

For the subset of 1000 points, the difference between the CCSD(T)/CBS and the MP2/aug-cc-pVDZ dispersion/repulsion energies is fitted to give a difference potential. In the pure fluorinated methane dimers, the CCSD(T)/CBS energy is lower than the MP2/aug-cc-pVDZ energy for all 1000 points. This is also the case for the HFC/CO_2 dimers, with the exception of 20–30 points on the repulsive wall. The difference parameters are fitted by a least-squares fit with all 1000 points equally weighted. A weighting toward the most stable structures is effectively included in the initial selection of the geometries. This fitted difference potential is added to the MP2/aug-cc-pVDZ fitted potential to give an effective CCSD(T)/CBS potential. The difference potential between the MP2/aug-cc-pVDZ and CCSD(T)/CBS interaction energies varies more smoothly than the total energy and is fitted with a rms error of about $30\mu E_h$ for all dimers, compared to an error of 200–$300\mu E_h$ for the whole potential energy surface (Tables II and III).

The second virial coefficient of a compound depends entirely on its pairwise interactions and, therefore, is a good test of the pair potential. The virial coefficients are calculated from the classical formula by evaluating the integral,

$$B_2 = -\frac{1}{2}\int \left\langle e^{-U_{12}/k_BT} - 1\right\rangle_{\Omega_1,\Omega_2} d\mathbf{R}, \tag{11}$$

where U_{12} is the pair potential and $\langle\cdots\rangle_{\Omega_1,\Omega_2}$ is the average over all orientations.

The nonadditive dispersion energy is calculated with SAPT using the random phase approximation (RPA) at the RPA/aug-cc-pVTZ level for a set of 250 trimers of each of CH_3F and CH_2F_2. The geometries of these trimers are chosen from simulations of the liquid phase. From a random time

TABLE VII. Second virial coefficients of the fluorinated methane-CO_2 dimers. Virial coefficients are in $cm^3\ mol^{-1}$.

	CH_3F/CO_2		CH_2F_2/CO_2	
T / K	Exp.[20]	Calc.	Exp.[21]	Calc.
303.15	–147.3	–132.0	–154.5	–188.3
313.15	–130.4	–122.0	–147.4	–174.5
323.15	–120.7	–113.1	–137.6	–162.1
333.15	–105.5	–105.0	–129.6	–151.1
343.15	–103.7	–97.6	–111.7	–140.9

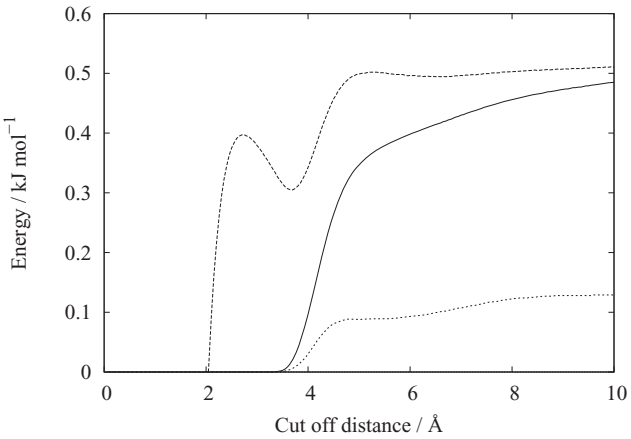

FIG. 1. Dispersion (solid line), dispersion with long-range correction (dashed line), and induction (dotted line) components of the nonadditive energy in CH_3F. Taken from a simulation of the liquid phase at 210 K.

step, a random molecule is selected. Then a second molecule is chosen with at least one atom within 4 Å of any in the first molecule. Finally, another molecule is chosen with any atom within 4 Å of an atom of either of the first two molecules. The nonadditive dispersion energies are fitted to the Axilrod–Teller equation (6). The Axilrod-Teller coefficients for trimers of like atoms, ν_{CCC}, ν_{FFF} and ν_{HHH}, are fitted to minimize the rms error in the energy and the ν coefficients for unlike interactions are generated assuming that

$$\nu^3_{abc} = \nu_{aaa}\nu_{bbb}\nu_{ccc}. \tag{12}$$

These fitted parameters reproduce the SAPT dispersion energies of both fluorinated methanes to within $3\mu E_h$ (Table IV). In these fits, the Axilrod–Teller coefficients for the central carbons are all zero. We find similar behavior for CO_2 (Ref. 7) and CH_4 (Ref. 8). In both of these cases, the distribution of the ν coefficients between the atoms does not affect the fitting error much, as long as the total ν for the whole molecule remains constant. We have shown empirically that the total nonadditive dispersion energy in simulations of CO_2 (Ref. 7) and CH_4 (Ref. 8) is approximately proportional to

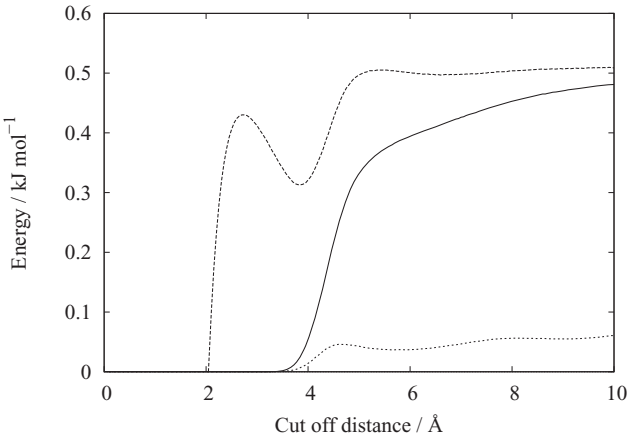

FIG. 2. Dispersion (solid line), dispersion with long-range correction (dashed line), and induction (dotted line) components of the nonadditive energy in CH_2F_2. Taken from a simulation of the liquid phase at 220 K.

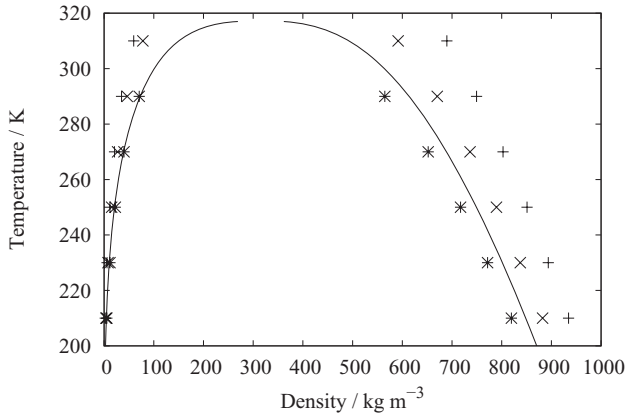

FIG. 3. The CH_3F phase-coexistence curve from experiment (Ref. 22) (solid line) and calculated using a pair potential (+), a pair potential with a correction for nonadditive dispersion (×), and a potential including the effects of nonadditive dispersion and nonadditive induction (*).

$k\rho^{2.5}$, where k is a constant. This approximation also holds for the fluorinated methanes and the proportionality constant k is fitted for each HFC (Table IV). The value of k for a mixture scales linearly between the values for the two components according to the mole fraction.

Nonadditive induction energies are calculated using SAPT at the RPA/aug-cc-pVTZ level for the sets of 250 trimers used for the nonadditive dispersion calculations. These are compared to three-body induction energies calculated using

$$U_{3,\mathrm{ind}} = \frac{1}{2}\sum_{a,b,c} -\mathbf{F}_{ab}\boldsymbol{\alpha}_b\mathbf{F}_{cb}, \tag{13}$$

where the polarizabilities, α, and charges and dipole moments used to generate the fields, $\mathbf{F}$, are taken from single-molecule calculations (Table I).

The phase-coexistence properties of the pure fluorinated methanes are simulated with the NVT Gibbs ensemble.[17] This ensemble simulates the liquid and vapor phases simultaneously, with volume and particle swap moves to equalize the pressure and chemical potential of the two phases. All simulations consist of 100 000 Monte Carlo passes, with the first 10 000 used to equilibrate the system. Each pass comprises, on average, one attempted rotation or translation move per molecule plus 150 attempted swap moves and one attempted volume move. Simulations are performed on 400 molecules, with the initial volume of the system chosen to ensure roughly equal distribution of these molecules between the two phases.

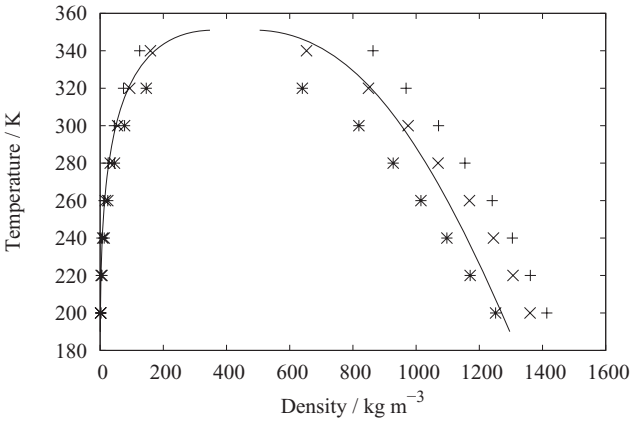

FIG. 4. The CH_2F_2 phase-coexistence curve from experiment (Ref. 22) (solid line) and calculated using a pair potential (+), a pair potential with a correction for nonadditive dispersion (×), and a potential including the effects of nonadditive dispersion and nonadditive induction (*).

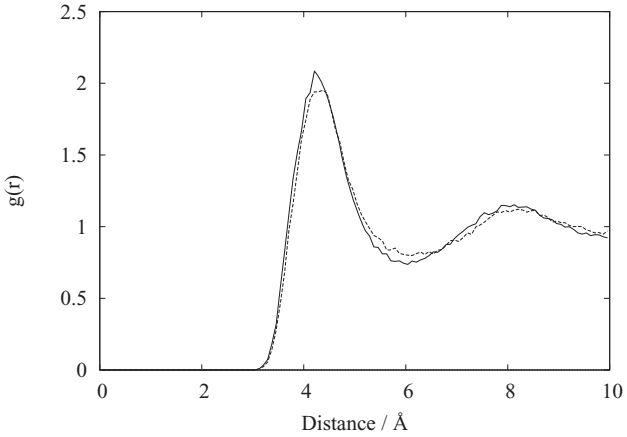

FIG. 5. The CH_2F_2 radial distribution function calculated at 220 K with nonpolarizable (solid) and polarizable (dashed) potentials.

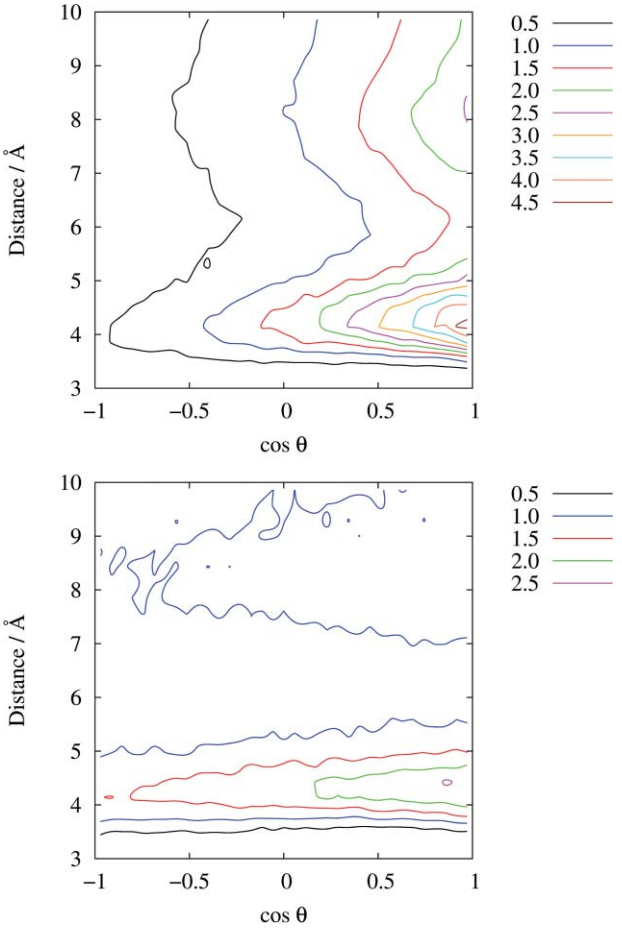

FIG. 6. The CH_2F_2 angular distribution function calculated at 220 K with nonpolarizable (top) and polarizable (bottom) potentials. θ is the angle between the molecular dipole moments of two molecules.

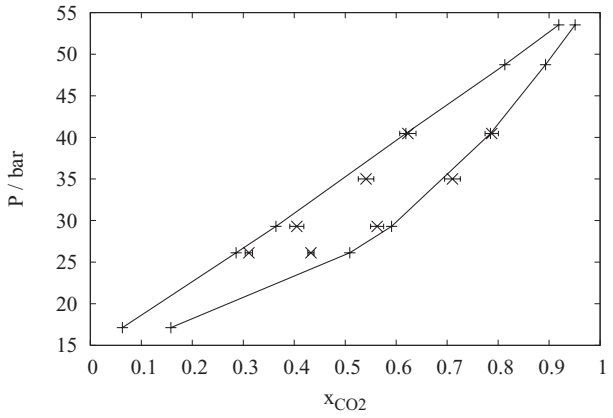

FIG. 7. The CH_2F_2/CO_2 phase-coexistence curve at 293 K. Experimental data (+ and solid lines) (Ref. 23) and calculations with nonadditive dispersion and induction included (×). Error bars are the uncertainties at the 95% confidence level.

The phase-coexistence curve of CH_2F_2/CO_2 is calculated with NPT Gibbs ensemble simulations.[18] We are unable to simulate the phase-coexistence curve of CH_3F/CO_2 because the coexistence envelope is very narrow and requires very large simulations to avoid finite-size effects.

Simulations using the nonpolarizable potentials only include the effect of pair induction. When polarizable potentials are used, the induction energy calculated with Eq. (3) includes both the two- and three-body components. The explicit inclusion of nonadditive dispersion in Gibbs ensemble simulations is computationally demanding. In simulations of CO_2 and CH_4, the nonadditive dispersion energy during a simulation correlates with $\rho^{2.5}$ and we use this approximation for all simulations presented here.[7]

IV. RESULTS

We compare the second virial coefficients of CO_2 calculated with our best pair potential (CBS-ad),[8] with those calculated with the empirical Trappe-EH potential[19] (Table V). The empirical potential reproduces the phase coexistence curve of CO_2, but underestimates the virial coefficients, because it implicitly includes multibody interactions as well as pair interactions. The CBS-ad potential reproduces the experimental virial coefficients to within 2 cm^3 mol^{-1}.

The calculated virial coefficients of the fluorinated methanes are compared with those measured by D'Amore and Di Nicola[20,21] (Table VI). The agreement between the calculated and experimental results is very good. The reproduction of the experimental virial coefficients of the mixed fluoromethane/CO_2 dimers is not as good as for the pure components (Table VII). However, the experimental values are obtained from average measurements over several mole fractions and have a larger error associated with them.

The nonadditive dispersion energies of the trimers of both fluorinated methanes vary between $-6\mu E_h$ and $80\mu E_h$. These energies are similar to those seen in CO_2 and CH_4. The Axilrod–Teller equation reproduces these energies with rms fitting errors of less than $3\mu E_h$ (Table IV). The parameters for both molecules are similar, which suggests that these parameters may be transferable to other HFCs. The best fits are seen with $\nu_{CCC} = 0$, which is probably caused by the absence of any trimers with close contacts involving carbon atoms. The nonadditive induction energies of the trimers vary over a larger range. They are between $-130\mu E_h$ and $200\mu E_h$ in CH_3F, and between $-150\mu E_h$ and $200\mu E_h$ in CH_2F_2. These sets of energies are both reproduced with rms errors of $21\mu E_h$ by Eq. (13).

The nonadditive dispersion and induction energy terms are evaluated on snapshots taken after every 1000 passes from simulations of the liquid phases of CH_3F (Fig. 1) and CH_2F_2 (Fig. 2). These energies are plotted with respect to a cutoff distance, using all trimers with at least two intermolecular separations less than this cutoff to calculate the nonadditive energies. When the long-range correction (7) is included, the nonadditive dispersion energy converges for cutoff radii greater than 6 Å. The nonadditive dispersion energy adds

TABLE VIII. The phase coexistence properties of CH_3F. Values in parentheses are the uncertainties at the 95% confidence level.

	Experiment	Nonpolarizable	Nonpolarizable + dispersion	Polarizable + dispersion
ΔH_{vap}^{210} / kJ mol^{-1}	15.85	18.02(0.07)	16.60(0.06)	14.94(0.05)
ΔH_{vap}^{250} / kJ mol^{-1}	13.25	16.03(0.04)	14.49(0.07)	12.59(0.08)
ΔH_{vap}^{290} / kJ mol^{-1}	9.19	13.46(0.06)	11.48(0.09)	8.90(0.12)
ρ_l^{210} / kg m^{-3}	848.7	934.5(2.0)	882.3(2.2)	819.5(2.9)
ρ_l^{250} / kg m^{-3}	750.0	851.1(2.7)	789.6(2.8)	717.3(3.1)
ρ_l^{290} / kg m^{-3}	612.5	759.5(4.5)	670.4(7.0)	569.5(10.3)
ρ_g^{210} / kg m^{-3}	4.6	2.3(0.2)	3.5(0.2)	5.5(0.3)
ρ_g^{250} / kg m^{-3}	20.7	11.8(0.5)	15.3(0.9)	22.5(1.1)
ρ_g^{290} / kg m^{-3}	73.2	35.1(1.8)	46.6(1.4)	69.1(3.1)
P_{210} / bar	2.2	1.2(0.1)	1.7(0.1)	2.6(0.1)
P_{250} / bar	10.2	6.5(0.3)	8.1(0.4)	11.3(0.5)
P_{290} / bar	31.7	19.9(0.8)	24.4(0.6)	31.9(0.9)

TABLE IX. The phase coexistence properties of CH_2F_2. Values in parentheses are the uncertainties at the 95% confidence level.

	Experiment	Nonpolarizable	Nonpolarizable + dispersion	Polarizable + dispersion
ΔH_{vap}^{220} / kJ mol^{-1}	19.95	23.00(0.07)	21.55(0.09)	17.79(0.19)
ΔH_{vap}^{260} / kJ mol^{-1}	17.41	20.05(0.13)	18.21(0.15)	14.79(0.07)
ΔH_{vap}^{300} / kJ mol^{-1}	13.9	15.70(0.29)	13.49(0.15)	10.81(0.10)
ρ_l^{220} / kg m^{-3}	1217	1362(3)	1308(4)	1171(8)
ρ_l^{260} / kg m^{-3}	1099	1240(6)	1169(6)	1015(4)
ρ_l^{300} / kg m^{-3}	953.2	1071(15)	959.8(11.8)	819.0(14.3)
ρ_g^{220} / kg m^{-3}	2.8	3.3(0.0)	3.2(0.2)	5.8(0.3)
ρ_g^{260} / kg m^{-3}	14.2	12.7(0.9)	16.9(0.6)	24.2(1.0)
ρ_g^{300} / kg m^{-3}	50.0	44.9(2.2)	54.7(3.2)	77.4(5.0)
P_{220} / bar	0.9	1.1(0.0)	1.1(0.1)	1.9(0.1)
P_{260} / bar	5.2	4.8(0.3)	6.2(0.2)	8.5(0.3)
P_{300} / bar	17.7	17.0(0.7)	19.6(0.9)	25.2(1.0)

a substantial repulsive interaction of about 0.5 kJ mol^{-1}. The nonadditive induction energy appears to be close to convergence at a cutoff of 10 Å. In both of the simulations considered here, the nonadditive induction energy contributes a repulsive interaction of about 0.1 kJ mol^{-1}.

The three-body dispersion and three-body induction terms both have a repulsive effect during Gibbs ensemble simulations. When only pair interactions are included in Gibbs ensemble simulations both fluorinated methanes are too strongly bound (Figs. 3 and 4, Tables VIII and IX). This leads to enthalpies of vaporization and liquid densities that are too large and gas densities that are too low. When nonadditive dispersion is included, a large repulsive interaction is added, leading to lower liquid densities and higher gas densities. This significantly improves the reproduction of the experimental phase-coexistence curves, but they are still too strongly bound. Including nonadditive induction adds another repulsive interaction, but in both CH_3F and CH_2F_2 the inclusion of both nonadditive terms leaves the liquid phase too weakly bound.

To understand the effect of nonadditive induction on the structure of the liquid, we plot the radial distribution function of CH_2F_2 calculated with polarizable and nonpolarizable potentials (Fig. 5). From this it is clear that the polarizable potential leads to a less ordered structure than the nonpolarizable potential. To understand the source of this disorder, we generated angular distribution functions using the methods described in our analysis[3] of simulations of CH_2F_2 with empirical potentials. The angular distribution function of CH_2F_2 (Fig. 6) shows that the atomic dipoles are strongly aligned when using a nonpolarizable potential. When nonadditive induction is included by using a polarizable potential, the molecular dipoles are more disordered. This accounts for the weaker binding in the liquid because the poorly aligned dipoles have weaker electrostatic interactions.

When calculating the phase-coexistence curve of CH_2F_2/CO_2 at 293 K, simulations without a nonadditive dispersion correction collapse into a single dense phase. When the effect of nonadditive dispersion is included, the phase-coexistence curve is reproduced well (Fig. 7). At pressures between 25 and 40 bar the molar ratios in both the liquid and gas phases are correct to within 0.1. Outside of this range finite size effects become important and larger simulations are needed to give good results.

V. CONCLUSION

We have shown that potentials fitted to high-quality *ab initio* dimer potential energy surfaces model their pairwise interactions of CO_2 and fluorinated methanes very well. The reproduction of the experimental second virial coefficients is good evidence that the pair interactions are modeled correctly. When these potentials are used to simulate phase-coexistence properties, the liquid phase is too strongly bound when only pairwise interactions are included. The inclusion of nonadditive dispersion and induction provides a substantial repulsive interaction and leads to much closer agreement with the experimental phase-coexistence curves. Some of the parameters in these potentials are transferable and could be used in simulations of other hydrofluorocarbons, and it is worth investigating whether potentials can be made where all the parameters can be transferred. Such potentials could be used to model refrigerants like R134a (Ref. 24) or larger fluorinated alkanes.

ACKNOWLEDGMENTS

We thank the Engineering and Physical Sciences Research Council for funding (Grant Nos. EP/E06082X/1 and EP/H024905/1) and the University of Nottingham High-Performance Computing facility for providing the computer resources used in this study. We also thank Dr. Allan Harvey for providing information on the experimental virial coefficients.

[1]M. Poliakoff and P. King, Nature **412**, 125 (2001).
[2]S. Higashi and A. Takada, Mol. Phys. **92**, 641 (1997).
[3]H. Do, R. J. Wheatley, and J. D. Hirst, J. Phys. Chem. B **114**, 3879 (2010).
[4]B. J. Palmer and J. L. Anchell, J. Phys. Chem. **99**, 12239 (1995).
[5]M. Tafazzoli and A. Khanlarkhani, J. Supercrit. Fluids **40**, 40 (2007).
[6]A. K. Sum and S. I. Sandler, Mol. Phys. **100**, 2433 (2002).
[7]M. T. Oakley and R. J. Wheatley, J. Chem. Phys. **130**, 034110 (2009).
[8]M. T. Oakley, H. Do, and R. J. Wheatley, Fluid Phase Equilibr. **290**, 48 (2010).
[9]T. C. Lillestolen and R. J. Wheatley, Chem. Commun. (Cambridge) **2008**, 5909.
[10]T. C. Lillestolen and R. J. Wheatley, J. Chem. Phys. **131**, 144101 (2009).
[11]M. P. Allen and D. J. Tildesley, *Computer Simulation of Liquids* (Clarendon, Oxford, 1987).
[12]T. C. Lillestolen and R. J. Wheatley, J. Phys. Chem. A **111**, 11141 (2007).
[13]B. M. Axilrod and E. Teller, J. Chem. Phys. **11**, 299 (1943).
[14]R. J. Wheatley and M. T. Oakley (unpublished).
[15]MOLPRO, a package of *ab initio* programs designed by H.-J. Werner and P. J. Knowles, version 2006.1, R. D. Amos, A. Bernhardsson, A. Berning, *et al.*
[16]K. A. Peterson, R. A. Kendall, and T. H. Dunning, J. Chem. Phys. **99**, 1930 (1993).
[17]A. Z. Panagiotopoulos, Mol. Phys. **61**, 813 (1987).
[18]A. Z. Panagiotopoulos, N. Quirke, M. Stapleton, and D. J. Tildesley, Mol. Phys. **63**, 527 (1988).
[19]B. Chen and J. I. Siepmann, J. Phys. Chem. B **103**, 5370 (1999).
[20]A. D'Amore, G. Di Nicola, F. Polonara, and R. Stryjek, J. Chem. Eng. Data **48**, 440 (2003).
[21]G. Di Nicola, F. Polonara, and R. Stryjek, J. Chem. Eng. Data **47**, 876 (2002).
[22]E. W. Lemmon, M. O. McLinden, and D. G. Friend, National Institute of Standards and Technology, Gaithersburg, July 7, 2009; available at http://webbook.nist.gov.
[23]F. Rivollet, A. Chapoy, C. Coquelet, and D. Richon, Fluid Phase Equilibr. **218**, 95 (2004).
[24]H. Do, R. J. Wheatley, and J. D. Hirst, Phys. Chem. Chem. Phys. **12**, 13266 (2010).